

PION PRODUCTION IN 650-MeV p-p COLLISIONS

V. M. GUZHAVIN, G. K. KLIGER, V. Z. KOLGANOV, A. V. LEBEDEV, K. S. MARISH, Yu. D. PROKOSHKIN, V. T. SMOLYANKIN, A. P. SOKOLOV, L. M. SOROKO, and TS'UI WA-CH'UANG

Institute of Theoretical and Experimental Physics; State Atomic Energy Commission (Erevan); Joint Institute for Nuclear Research

Submitted to JETP editor November 14, 1963

J. Exptl. Theoret. Phys. (U.S.S.R.) 46, 1245-1256 (April, 1964)

The angular and energy distributions of pions produced by 650-MeV protons and pion-nucleon correlations were studied using a liquid hydrogen bubble chamber. The present investigation indicates that the experimental angular distributions of neutral and charged pions are consistent with the assumption of isotopic spin conservation. The contributions of  $\pi N$  subsystem states with isospin  $T_{\pi N} = 1/2$  and  $3/2$  are measured; the contribution of the latter is  $72 \pm 3\%$ .

INTRODUCTION

INTENSIVE investigations of pion production by 600-MeV nucleons in the meson-nucleon resonance region ( $T_{\pi N} = 3/2, J_{\pi N} = 3/2$ ) have determined the quantitative characteristics of all meson production processes and have made possible the construction of a phenomenological resonance model agreeing with experiment.<sup>[1]</sup> However, several questions have remained unanswered, among them the possibility that isospin is not conserved<sup>[2]</sup> and the role of ( $3/2, 3/2$ ) resonance in pion production.

In the given energy region there is practically no production of pion pairs, but the following four proton-proton processes can occur:

- $p + p \rightarrow p + p,$  (1)
- $p + p \rightarrow d + \pi^+,$  (2)
- $p + p \rightarrow p + n + \pi^+,$  (3)
- $p + p \rightarrow p + p + \pi^0.$  (4)

The angular distributions of pions in reactions (2)–(4) at about 600 MeV are well approximated by second-degree polynomials of the form<sup>1)</sup>

$$f(\theta_\pi) \sim 1/3 + b_\pi \cos^2 \theta_\pi. \tag{5}$$

If isospin is conserved the total angular distributions of the neutral and charged pions produced in proton collisions with protons and neutrons should be identical:

$$f_{pp+pn}(\theta_{\pi^0}) = f_{pp+pn}(\theta_{\pi^\pm}), \tag{6}$$

which is equivalent to

<sup>1)</sup>Unless otherwise specified, the kinematic characteristics of the reactions (angles, momenta, and energies) will always pertain to the center-of-mass system of the colliding nucleons.

$$b_{\pi^0} = b_{\pi^\pm}. \tag{7}$$

The angular distribution of neutron pions produced in p-p and p-n collisions at about 650 MeV, taking into account the  $\pi^0$  energy spectra,<sup>[3]</sup> is almost isotropic:

$$b_{\pi^0} = 0.22 \pm 0.05. \tag{8}$$

Much more anisotropy was found in the angular distribution for the principal charged-pion production reaction (3); this was observed in the first investigations of the process:<sup>[4] 2)</sup>

$$f_{pp \rightarrow pn\pi^+}(\theta_{\pi^+}) \sim 1/3 + (0.51 \pm 0.11) \cos^2 \theta_{\pi^+}. \tag{9}$$

The other reactions make only a small contribution to (7). When (9) is used to calculate  $b_{\pi^\pm}$  the ratio  $b_{\pi^0}/b_{\pi^\pm}$  is considerably smaller than unity:

$$b_{\pi^0}/b_{\pi^\pm} = 0.44 \pm 0.12.$$

This led to the conclusion<sup>[2]</sup> that either isospin is not conserved in the given energy region or (9) is incorrect. The latter conclusion was supported by spectrometric data<sup>[6]</sup> which disagree with (9):

$$f_{pp \rightarrow pn\pi^+}(\theta_{\pi^+}) \sim 1/3 + (0.03 \pm 0.08) \cos^2 \theta_{\pi^+}.$$

The value of  $b_{\pi^\pm}$  obtained by using this last distribution is close to that of  $b_{\pi^0}$ :  $b_{\pi^0}/b_{\pi^\pm} = 1.3 \pm 0.6$ .

Because of the foregoing discrepancy it has been emphasized several times<sup>[2,7]</sup> that the angular distribution for reaction (3) must be obtained more accurately. It was one of the aims of the present work to measure this distribution by a direct method not requiring essential corrections

<sup>2)</sup>See in [4] the remark regarding earlier measurements by means of photographic emulsions.<sup>[5]</sup>

to the measured quantities, such as cannot be avoided when reaction (3) is investigated with scintillation counters.

It was another purpose of our investigation to determine the role of ( $3/2, 3/2$ ) resonance in pion production processes. Mandelstam's resonance model<sup>[1]</sup> has accounted quantitatively for most experimental findings regarding pion production in p-p collisions at about 600 MeV on the basis of the hypothesis that the  $\pi N$  subsystem consists very predominantly of states with isospin  $T_{\pi N} = 3/2$ .

It follows from this hypothesis that in the given energy region there should be no appreciable production of pions by nucleons in states with zero total isospin; this conflicted with experiment.<sup>[8]</sup> Mandelstam's resonance model was therefore, at the very least, incomplete and an experimental test of his initial assumptions was required, i.e. the determination of the probability ratio of  $\pi N$  subsystem production in the states with  $T_{\pi N} = 3/2$  and  $1/2$ . It was suggested in<sup>[9]</sup> that this ratio could be determined by utilizing the symmetry of wave functions in isospin space with respect to the exchange of the two secondary nucleons in reaction (3).

The cross sections for processes (3) and (4) are determined by the two isospin amplitudes  $A_{13}$  and  $A_{11}$ . The first index is the isospin of the two nucleons in the initial state, while the second index is  $2T_{\pi N}$ . In order to solve the inverse problem, i.e. to determine experimentally the amplitudes  $A_{13}$  and  $A_{11}$  and the phase angles between them, three independent cross sections must be measured. Two of these, the cross sections for (2) and (4), had been measured previously. The third quantity is the cross section difference  $\Delta\sigma$ , characterizing the spatial asymmetry in (3) with regard to the exchange of the neutron and proton.<sup>[9]</sup>

If we confine ourselves to the S and P waves of the  $\pi^+$  meson and secondary nucleons, the interference term associated with this asymmetry in the cross section difference has the form

$$a(p_{\pi^+}) \cos \theta_{\pi^+} \cos \theta_{12}, \quad (10)$$

where the angle  $\theta_{12}$  is the direction of neutron emission in the c.m. system of secondary nucleons with respect to the  $\pi^+$  momentum (Fig. 1), and  $p_{\pi^+}$  is the  $\pi^+$  momentum. The sign of the interference term (10) is reversed when we make the substitution  $\theta_{\pi^+} \rightarrow 180^\circ - \theta_{\pi^+}$  or  $\theta_{12} \rightarrow 180^\circ - \theta_{12}$ . Therefore the cross section difference  $\Delta\sigma$  is measured separately in the regions  $0 < \theta_{\pi^+} < 90^\circ$  and  $90^\circ < \theta_{\pi^+} < 180^\circ$  or  $0 < \theta_{12} < 90^\circ$  and  $90^\circ < \theta_{12} < 180^\circ$ .

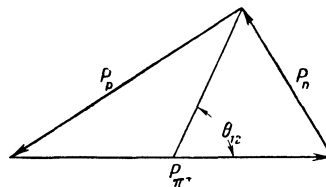


FIG. 1. Kinematics of reaction (3).  $p_p$ ,  $p_n$ , and  $p_{\pi^+}$  are the momenta of the proton, neutron, and  $\pi^+$  meson.

When  $\Delta\sigma$  has been obtained, the isospin amplitudes and phase angle  $\omega_{13,11}$  between them are determined from

$$\begin{aligned} |A_{13}|^2 &= \frac{2}{3} \sigma(pp \rightarrow pn\pi^+) + \frac{2}{3} \Delta\sigma, \\ |A_{11}|^2 &= \sigma(pp \rightarrow pp\pi^0) + \frac{1}{3} \sigma(pp \rightarrow pn\pi^+) - \frac{2}{3} \Delta\sigma, \\ 3 |A_{13}| |A_{11}| \cos \omega_{13,11} &= \sqrt{2} [3\sigma(pp \rightarrow pp\pi^0) \\ &\quad - \sigma(pp \rightarrow pn\pi^+)] + \frac{1}{\sqrt{2}} \Delta\sigma. \end{aligned} \quad (11)$$

In order to solve the aforementioned problem we must have complete simultaneous experimental information concerning the three particles in the final state. The necessary experiment could only be performed by means of a "track chamber."

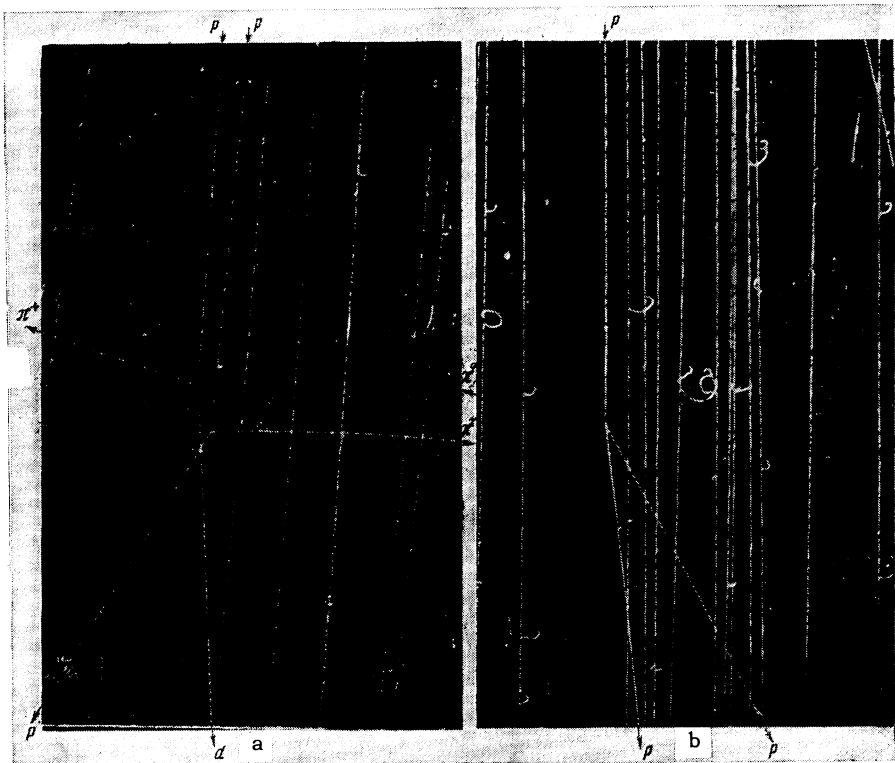
In the present work proton interactions were investigated using a liquid hydrogen bubble chamber, which enabled us to obtain a complete kinematic picture of processes (1)–(4). It was thus possible not only to determine the cross sections, angular distributions, and energy spectra of the particles by a method that was free of the systematic errors present in experiments utilizing counters, but also to obtain information regarding angular and energy correlations of particles in the three-particle processes (3) and (4). We thus observed the characteristics of meson production which could not be measured using the earlier technique. Finally, an important advantage of the liquid hydrogen bubble chamber technique is the possibility of studying all p-p scattering processes in a single experiment, thus considerably enhancing the reliability of the data.

## MEASURING PROCEDURE

The experiments now to be described were performed in 1961–62 using a 650-MeV proton beam from the synchrocyclotron at the Laboratory for Nuclear Problems of the Joint Institute for Nuclear Research. At the same time similar experiments were being performed at a lower energy by an Italian group using a CERN bubble chamber.<sup>[10]</sup>

The proton beam extracted from the synchro-

FIG. 2. Typical photographs of the events. a -  $p + p \rightarrow d + \pi^+$  and  $p + p \rightarrow p + n + \pi^+$ ; b -  $p + p \rightarrow p + p + \pi^0$



cyclotron was defined by a deflecting magnet and collimator system and was directed into the center of the bubble chamber by means of a quadrupole positioning lens. The proton beam intensity was monitored by a scintillation counter ahead of the bubble chamber; the count was 10–20 protons per pulse, i.e., about  $10^{-6}$  of the total beam intensity. The liquid hydrogen bubble chamber (of the Institute of Theoretical and Experimental Physics) used in our experiments had a diameter of 13 cm and was placed in a 13-kOe magnetic field. Particle tracks in the chamber were photographed by a stereo camera synchronized with the synchrocyclotron.

About 3200 proton interactions were observed in 25,000 scanned stereo photographs. Events were identified by measuring the track coordinates with semiautomatic equipment; this was followed by processing of the data on an electronic computer, and also by measuring space angles in reprojection. The average accuracy of the measured momenta and space angles  $\theta$  and  $\varphi$  was determined by analyzing the photographs of two-particle events (1) and (2), whose kinematic characteristics can be calculated accurately; the results were

$$\Delta p = 20\%, \quad \Delta\theta = 1^\circ, \quad \Delta\varphi = 3^\circ.$$

The angle  $\theta_{12}$  was measured to within  $20^\circ$ .

Elastic and inelastic proton interactions were separated by comparing the measured and calcu-

lated momenta and angles. Another test of correct event identification was provided by evaluating the amount of ionization along tracks. The three-particle reactions (3) and (4) were also separated by means of kinematic analysis. Only about 2% of the events could not be interpreted uniquely; typical photographs of events are shown in Fig. 2.

### CROSS SECTIONS

In determining the total cross section  $\sigma_t$  for proton interactions a central region was defined in the chamber in order to avoid errors associated with scanning losses. Simultaneously with the 2444 proton interactions observed in this region, the number of protons (183,000) traversing the chamber was counted. The total cross section was obtained from the known density of liquid hydrogen, with small corrections for scanning inefficiency:

$$\sigma_t = (41.8 \pm 1.1) \cdot 10^{-27} \text{ cm}^2.$$

Elastic scatterings comprise  $60 \pm 2\%$  of the aforementioned total number of interactions. The cross sections for elastic ( $\sigma_s$ ) and inelastic ( $\sigma_a$ ) scattering are

$$\sigma_s = (25.1 \pm 0.8) \cdot 10^{-27} \text{ cm}^2, \quad \sigma_a = (16.7 \pm 0.6) \cdot 10^{-27} \text{ cm}^2.$$

To determine the cross sections for reactions (2)–(4) a narrower region of the chamber was defined for study. The process of event identification

in this region yielded the following results:

Reaction	(2)	(3)	(4)	(2) or (4)	(3) or (4)
No. of events	113	430	118	5	9

Following some small corrections for scanning inefficiency, we obtained the following cross sections for processes (2)–(4):

$$\sigma(pp \rightarrow pn\pi^+) = (10.8 \pm 0.5) \cdot 10^{-27} \text{ cm}^2,$$

$$\sigma(pp \rightarrow pp\pi^0) = (3.0 \pm 0.3) \cdot 10^{-27} \text{ cm}^2,$$

$$\sigma(pp \rightarrow d\pi^+) = (2.9 \pm 0.3) \cdot 10^{-27} \text{ cm}^2.$$

All the foregoing cross sections agree well with earlier values.<sup>[4,11-14]</sup>

#### THE REACTION $p + p \rightarrow d + \pi^+$

The angular distribution of  $\pi^+$  mesons produced in process (2) is shown in Fig. 3; the experimental distribution has been corrected slightly for scanning inefficiency at small angles  $\theta_{\pi^+}$ . The measured angular distribution is symmetric about  $\theta_{\pi^+} = 90^\circ$ ; this indicates the absence of appreciable systematic errors in determining  $\pi^+$  yields at different angles. The observed angular distribution for reaction (2) is well approximated by a second-degree polynomial:

$$f_{pp \rightarrow d\pi^+}(\theta_{\pi^+}) \sim 1/3 + (1.22 \pm 0.25) \cos^2 \theta_{\pi^+}. \quad (12)$$

This distribution is in good agreement with earlier experimental results.<sup>[14]</sup>

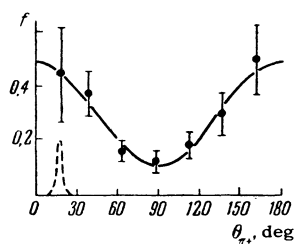


FIG. 3. Angular distribution of  $\pi^+$  mesons from the reaction  $p + p \rightarrow d + \pi^+$ . The ordinates in all graphs represent arbitrary units. The curve is the normalized polynomial (12). The dashed curve shows the angular resolution.

#### THE REACTION $p + p \rightarrow p + n + \pi^+$ AND ISOSPIN CONSERVATION

Figure 4 shows that the angular distribution of  $\pi^+$  mesons from the reaction (3). This distribution is also seen to be symmetric. A polynomial approximating the differential cross section was obtained by least squares:

$$\frac{d\sigma}{d\Omega}(pp \rightarrow pn\pi^+) = [(0.68 \pm 0.05)$$

$$+ (0.51 \pm 0.15) \cos^2 \theta_{\pi^+}] \cdot 10^{-27} \text{ cm}^2/\text{sr}, \quad (13)$$

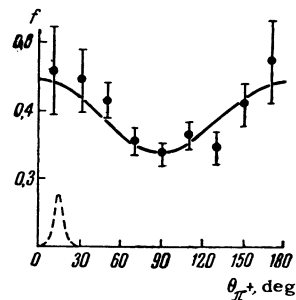


FIG. 4.  $\pi^+$  angular distribution in  $p + p \rightarrow p + n + \pi^+$ . The curve is the normalized polynomial (14). The dashed curve shows the angular resolution.

or, as represented by (5),

$$f_{pp \rightarrow pn\pi^+}(\theta_{\pi^+}) \sim 1/3 + (0.25 \pm 0.07) \cos^2 \theta_{\pi^+}. \quad (14)$$

The distribution (14) was considerably closer to isotropy than that given in<sup>[4]</sup>. This discrepancy appears to be due to the fact that the angular distribution given in<sup>[4]</sup> was measured with a detector having its threshold at approximately 70 MeV for  $\pi^+$  registration; to determine the total  $\pi^+$  yield the energy spectrum was extrapolated to lower energies on the basis of certain assumptions. From our present measurements of the  $\pi^+$  spectrum, which were not limited by any energy threshold, we find that the mean  $\pi^+$  energy is 95 MeV, with one-third of the  $\pi^+$  mesons having energies below 70 MeV. As shown in Fig. 5, the actual  $\pi^+$  spectrum was found to be softer than in<sup>[4]</sup>. The distribution (14) also differs from the isotropic distribution given in<sup>[6]</sup>.

The total angular distribution of  $\pi^+$  mesons produced in the reactions (2) and (3) is represented by

$$f_{pp}(\theta_{\pi^+}) \sim 1/3 + (0.38 \pm 0.07) \cos^2 \theta_{\pi^+}. \quad (15)$$

Utilizing data concerning the angular distribution of charged pions produced in n-p collisions,<sup>[15]</sup> we obtain

$$b_{\pi^\pm} = 0.32 \pm 0.07.$$

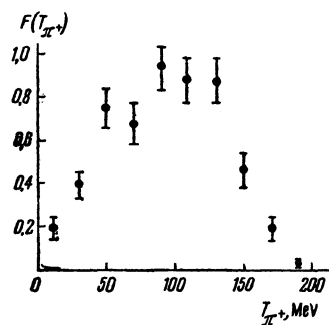


FIG. 5.  $\pi^+$  energy distribution in  $p + p \rightarrow p + n + \pi^+$ .

Comparing this result with  $b_{\pi^0}$  of (8), we find that isospin conservation (7) is not violated at 650 MeV:

$$b_{\pi^0}/b_{\pi^\pm} = 0.7 \pm 0.2.$$

### THE RELATION BETWEEN ANGLE AND ENERGY VARIABLES

The  $\pi^+$  distribution for reaction (3) in the investigated region is

$$f(\theta_{\pi^+}, T_{\pi^+}) = a(T_{\pi^+})^{1/3} + b(T_{\pi^+}) \cos^2 \theta_{\pi^+}, \quad (16)$$

where the coefficient  $b$  is in general dependent on the  $\pi^+$  energy  $T_{\pi^+}$ , i.e. the  $\pi^+$  energy spectrum can vary with the angle  $\theta_{\pi^+}$ . In order to determine whether there is any correlation between the angle and energy variables in (16), the  $\pi^+$  energy spectra were constructed for two intervals of  $\theta_{\pi^+}$ . As shown by the table, these spectra were similar. Unlike the result in [4], the tabulated data show a separation of the energy and angle variables in (16):

$$b(T_{\pi^+}) \approx \text{const.}$$

$T_{\pi^+}$ MeV (interval)	No. of events		$\frac{N(\cos^2 \theta_{\pi^+} < 1/2)}{N(\cos^2 \theta_{\pi^+} > 1/2)}$
	$N(\cos^2 \theta_{\pi^+} > 1/2)$	$N(\cos^2 \theta_{\pi^+} < 1/2)$	
0-20	4	10	$1.8 \pm 0.5$
20-40	11	17	
40-60	18	34	
60-80	13	33	$2.2 \pm 0.4$
80-100	18	52	$1.9 \pm 0.3$
100-120	26	31	
120-140	28	41	
140-160	11	27	$1.7 \pm 0.3$
160-180	0	1	
0-180	129	246	$1.9 \pm 0.2$
Mean energy, MeV	$93 \pm 5$	$90 \pm 5$	

### DETERMINATION OF CONTRIBUTIONS FROM STATES WITH $T_{\pi N} = 3/2$ AND $1/2$

Figure 6 shows the distribution of events with respect to the angles  $\theta_{12}$  and  $\theta_{\pi^+}$  in reaction (3). As expected from the resonance model, these distributions are asymmetric, with opposite asymmetry signs, in accordance with (10), for the two regions  $\theta_{\pi^+} < 90^\circ$  and  $\theta_{\pi^+} > 90^\circ$ . It also follows from Fig. 6 that the interference term in the cross section actually has the form (10), i.e., the asymmetry is not affected by the exchange  $\theta_{\pi^+} \leftrightarrow \theta_{12}$ .

Adding the distributions shown in Fig. 6a (with allowance for the angular resolution), i.e., calculating the numbers of events:

$$\begin{aligned} N_1 &= N(\theta_{\pi^+} < 90^\circ, \theta_{12} < 90^\circ) + N(\theta_{\pi^+} > 90^\circ, \theta_{12} > 90^\circ), \\ N_2 &= N(\theta_{\pi^+} < 90^\circ, \theta_{12} > 90^\circ) + N(\theta_{\pi^+} > 90^\circ, \theta_{12} < 90^\circ), \end{aligned} \quad (17)$$

we find that  $N_1 = 244$  and  $N_2 = 129$ . We have, by definition,

$$\Delta\sigma = [(N_1 - N_2)/(N_1 + N_2)] \sigma(pp \rightarrow pn\pi^+),$$

so that

$$\Delta\sigma = (3.4 \pm 0.6) \cdot 10^{-27} \text{ cm}^2. \quad (18)$$

From (11) we obtain

$$|A_{13}|^2 = (9.6 \pm 0.8) \cdot 10^{-27} \text{ cm}^2,$$

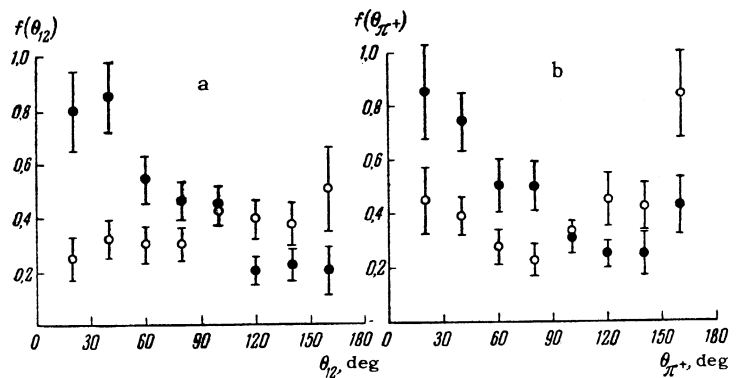
$$|A_{11}|^2 = (3.9 \pm 0.5) \cdot 10^{-27} \text{ cm}^2. \quad (19)$$

The relative phase angle  $\omega_{13,11}$  is close to  $90^\circ$ :

$$\cos \omega_{13,11} = -0.1 \pm 0.1,$$

i.e., there is practically no interference between the states with  $T_{\pi N} = 3/2$  and  $1/2$ . To calculate  $|A_{11}|$ , in place of the reaction for reaction (4) measured at 650 MeV we used the value of  $\sigma^*(pp \rightarrow pp\pi^0)$  obtained from  $\sigma(pp \rightarrow pp\pi^0)$  by introducing a small correction for the difference

FIG. 6. a -  $\theta_{12}$  distribution of  $p + p \rightarrow p + n + \pi^+$  events:  $\bullet$  -  $\theta_{\pi^+} < 90^\circ$ ,  $\circ$  -  $\theta_{\pi^+} > 90^\circ$ ; b -  $\theta_{\pi^+}$  distribution of  $p + p \rightarrow p + n + \pi^+$  events:  $\bullet$  -  $\theta_{12} < 90^\circ$ ,  $\circ$  -  $\theta_{12} > 90^\circ$ .



between the maximum pion momenta in reactions (3) and (4), which is associated with the difference between the masses of charged and neutral mesons and the nucleonic mass.

Figure 7 shows the region of possible values of  $k^2 = |A_{13}|^2/|A_{11}|^2$  and  $\alpha = \sigma(pp \rightarrow pn\pi^+)/\sigma^*(pp \rightarrow pp\pi^0)$  and indicates the values obtained in the present work (taking into account the results of earlier investigations<sup>[13]</sup>):

$$k^2 = 2.5 \pm 0.3, \quad \alpha = 4.1 \pm 0.4.$$

Thus the  $\pi N$  subsystem in reactions (3) and (4) is formed mainly in states with  $T_{\pi N} = 3/2$ . At the same time, however, by contrast with Mandelstam's

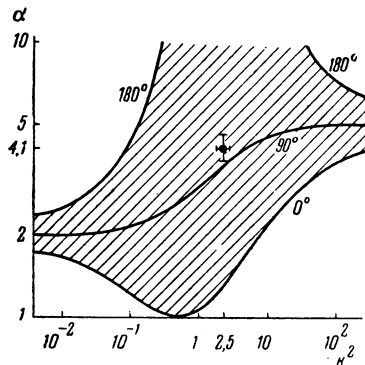


FIG. 7.  $k^2$  versus  $\alpha$ . ● — our result. The shaded region contains the possible values of  $k^2$  and  $\alpha$ . Values of  $\omega_{13,11}$  are indicated on the curves.

$p_p$ , MeV/c:	0 — 150	150 — 300	300 — 480	Average over the spectrum
$N_1/N_2$ :	$2.1 \pm 0.6$	$1.5 \pm 0.2$	$2.0 \pm 0.3$	$1.9 \pm 0.2$

It is evident from the ratios  $N_1/N_2$  characterizing the asymmetry of the distribution  $f(\theta_{12})$  that the ratio between the contributions of states with  $T_{\pi N} = 3/2$  and  $1/2$  has little dependence on the energy of the secondary proton.

The asymmetry of  $f(\theta_{12})$  is only slightly dependent on the  $\pi^+$  energy:

$T_{\pi^+}$ , MeV:	0 — 70	70 — 120	> 120
$N_1/N_2$ :	$1.8 \pm 0.3$	$1.8 \pm 0.3$	$2.1 \pm 0.4$

#### TRANSITIONS WITH LARGE ORBITAL ANGULAR MOMENTA

Figure 10 shows the angular distributions of protons in reaction (3) for large and small values of the momentum  $p_p$ . As was to be expected, the distribution of low-energy protons is well fitted by a second-degree polynomial, i.e., only the S and P proton states are important in this case. In the case of high-energy protons, which experience predominantly a large momentum transfer,

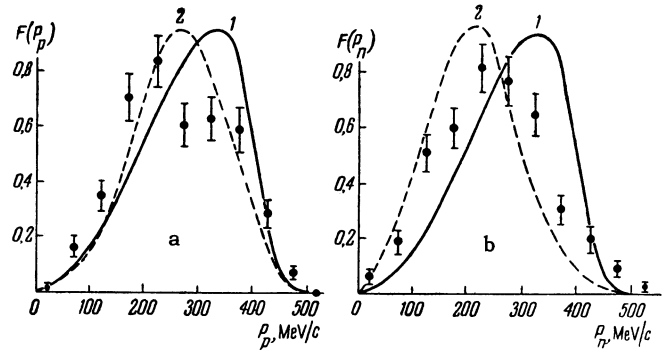


FIG. 8. Momentum distributions of (a) protons and (b) neutrons in  $p + p \rightarrow p + n + \pi^+$ . The (1) statistical and (2) resonance distributions were calculated allowing for the resolving power of the apparatus.

model, we observe a fairly intense production of  $\pi N$  subsystems in states with  $T_{\pi N} = 1/2$ .

Figures 8 and 9 show the momentum distributions, obtained in the present work, of nucleons in reaction (3) and the distribution of the relative kinetic energy  $Q_{N\pi^+}$  of  $\pi^+$  and one nucleon.

In order to determine how the contribution ratio of states with  $T_{\pi N} = 3/2$  and  $1/2$  varies as the secondary-proton energy increases, all registered instances of reaction (3) were divided into three groups corresponding to different values of the secondary-proton momentum  $p_p$ . The  $\pi^+$  distribution with respect to the angle  $\theta_{12}$  was obtained for each group:

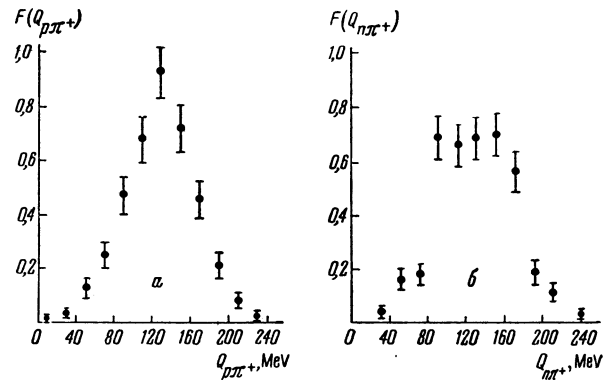


FIG. 9. Distributions with respect to  $Q_{N\pi^+}$  of subsystems (a)  $\pi^+$ -proton and (b)  $\pi^+$ -neutron in  $p + p \rightarrow p + n + \pi^+$ .

the angular distribution curve rises rapidly in the region  $\cos^2\theta_p \approx 1$ . This appears to indicate the presence of secondary protons with orbital angular momentum  $l > 1$ . The cross section for these transitions does not exceed  $0.5 \times 10^{-27} \text{ cm}^2$ .

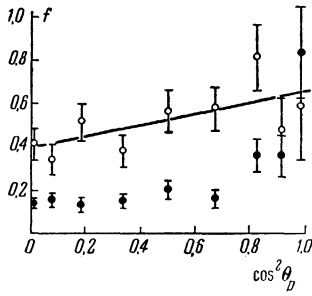


FIG. 10

FIG. 10. Angular distributions of protons in  $p + p \rightarrow p + n + \pi^+$  for two proton groups:  $\circ - p_p < 275$  MeV/c,  $\bullet - p_p > 275$  MeV/c. The straight line is the normalized polynomial  $\frac{1}{3} + 0.21 \cos^2 \theta_p$ .

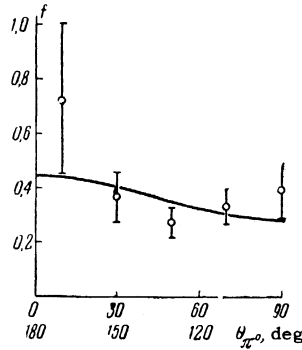


FIG. 11

FIG. 11. Angular distribution of  $\pi^0$  mesons in  $p + p \rightarrow p + p + \pi^0$ . The curve is the normalized polynomial (20).

THE REACTION  $p + p \rightarrow p + p + \pi^0$

The characteristics of the reaction (4) can be obtained with less accuracy than for charged pion production. Our  $\pi^0$  angular distribution (Fig. 11) is approximated by

$$f_{pp \rightarrow pp\pi^0}(\theta_{\pi^0}) \sim \frac{1}{3} + (0.04 \pm 0.015) \cos^2 \theta_{\pi^0}, \quad (20)$$

which agrees well with earlier isotropic angular distributions.<sup>[13,16]</sup> Our  $\pi^0$  energy spectrum (Fig. 12) agrees with Mandelstam's resonance model.<sup>[1]</sup>

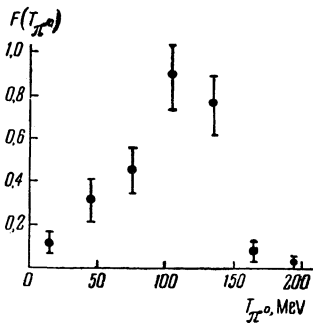


FIG. 12

FIG. 12. Energy spectrum of  $\pi^0$  mesons in  $p + p \rightarrow p + p + \pi^0$ .

FIG. 13. Angular distribution of secondary protons in  $p + p \rightarrow p + p + \pi^0$  ( $\bullet$ ). The curve is the normalized polynomial (21).  $\circ$  - distribution of secondary protons with  $p_p < 250$  MeV/c.

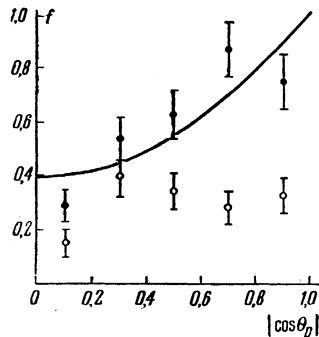


FIG. 13

Unlike the  $\pi^0$  distribution, the angular distribution of secondary protons in reaction (4) was anisotropic (Fig. 13), thus confirming the important role of states with total angular momentum  $J \geq 2$ .<sup>[13]</sup> The angular distribution is represented by

$$f_{pp \rightarrow pp\pi^0}(\theta_p) \sim \frac{1}{3} + (0.5 \pm 0.2) \cos^2 \theta_p. \quad (21)$$

The observed anisotropy of the angular distribution results mainly from high-energy protons. Figure 13 shows the almost isotropic angular distribution of low-energy secondary protons. The momentum spectrum of the secondary protons shown in Fig. 14 agrees with the hypothesis that states with  $T_{\pi N} = \frac{3}{2}$  predominate.

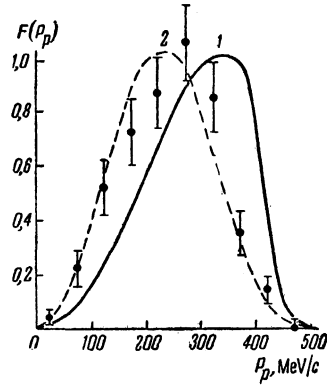
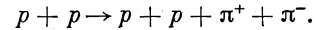


FIG. 14. Momentum spectrum of secondary protons in  $p + p \rightarrow p + p + \pi^0$ . Curve 1 - statistical distribution; curve 2 - resonance distribution calculated with allowance for the resolving power of the apparatus.

PION PAIR PRODUCTION

Scanning of the photographs revealed no four-pronged event which could be interpreted as pion pair production in the reaction



The estimated upper limit of the cross section for this reaction is

$$\sigma(pp \rightarrow pp\pi^+\pi^-) < 2 \cdot 10^{-29} \text{ cm}^2$$

In conclusion, we wish to thank the technicians and laboratory personnel who were responsible for the excellent operation of the liquid-hydrogen bubble chamber, the scanning group of the Institute of Theoretical and Experimental Physics headed by D. I. Tumanova, the scanning group of the Joint Institute for Nuclear Research, and E. M. Landis and E. S. Gal'pern for programming and operating the electronic computer.

<sup>1</sup>S. Mandelstam, Proc. Roy. Soc. (London) **A244**, 491 (1958).

<sup>2</sup>A. F. Dunaitsev and Yu. D. Prokoshkin, JETP **38**, 747 (1960), Soviet Phys. JETP **11**, 540 (1960).

<sup>3</sup>Lü Min and Yu. D. Prokoshkin, JETP **43**, 1202 (1962), Soviet Phys. JETP **16**, 851 (1963).

<sup>4</sup>B. S. Neganov and O. V. Savchenko, *JETP* **32**, 1265 (1957), *Soviet Phys. JETP* **5**, 1033 (1957).

<sup>5</sup>V. M. Sidorov, *JETP* **31**, 178 (1956), *Soviet Phys. JETP* **4**, 22 (1957).

<sup>6</sup>Meshkovskii, Shalamov, and Shebanov, *JETP* **35**, 64 (1958), *Soviet Phys. JETP* **8**, 46 (1959).

<sup>7</sup>Pontecorvo, Mukhin, Prokoshkin, and Soroko, *Trudy Mezhdunarodnoĭ konferentsii po fizike chastits vysokikh energii* (Trans. Intern. Conf. on Phys. High-Energy Particles) Vol. 1, Kiev, 1959.

<sup>8</sup>Yu. M. Kazarinov and Yu. N. Simonov, *JETP* **35**, 78 (1958), *Soviet Phys. JETP* **8**, 56 (1959); A. F. Dunaĭtsev and Yu. D. Prokoshkin, *JETP* **38**, 747 (1959), *Soviet Phys. JETP* **11**, 540 (1960); Yu. D. Prokoshkin, Preprint D-569, Joint Inst. Nuclear Res., 1960; Dzhelepov, Kiselev, Oganesyanyan, and Flyagin, Proc. 1960 Ann. Intern. Conf. on High-Energy Physics at Rochester, Univ. of Rochester, 1960, p. 46.

<sup>9</sup>K. S. Marish and L. M. Soroko, *JETP* **40**, 605 (1961), *Soviet Phys. JETP* **13**, 423 (1961).

<sup>10</sup>Baldoni, Focardi, Hromadik, Monari, Saporetta, Femino, Mezzanares, Bertolini, and Gialanella, *Nuovo cimento* **26**, 1376 (1962).

<sup>11</sup>Dzhelepov, Moskalev, and Medved', *DAN SSSR* **104**, 380 (1955).

<sup>12</sup>N. P. Bogachev and I. K. Vzorov, *DAN SSSR* **104**, 38 (1955).

<sup>13</sup>A. F. Dunaĭtsev and Yu. D. Prokoshkin, *JETP* **36**, 1656 (1959), *Soviet Phys. JETP* **9**, 1179 (1959).

<sup>14</sup>M. G. Meshcheryakov and B. S. Neganov, *DAN SSSR* **100**, 677 (1955).

<sup>15</sup>Dzhelepov, Kiselev, Oganesyanyan, and Flyagin, op. cit. reference [8].

<sup>16</sup>Yu. D. Bayukov and A. A. Tyapkin, *JETP* **32**, 953 (1957), *Soviet Phys. JETP* **5**, 779 (1957).

Translated by I. Emin  
179